Review

Journal of Photopolymer Science and Technology
Volume 28, Number 5 (2015) 635 – 642 ©2015SPST

Sub-20 nm Microphase-Separated Structures in Hybrid Block Copolymers Consisting of Polycaprolactone and Maltoheptaose

Takuya Isono,[†] Issei Otsuka,[‡] Sami Halila,[‡] Redouane Borsali,[‡] Toyoji Kakuchi,[†] and Toshifumi Satoh[†,*]

[†]*Division of Biotechnology and Macromolecular Chemistry, Faculty of Engineering, Hokkaido University*
Kita 13, Nishi 8, Kita-Ku, Sapporo 060-8628, Japan
[‡]*Centre de Recherches sur les Macromolécules Végétales*
BP53, 38041 Grenoble Cedex 9, France

The present review summarizes our recent results regarding the synthesis and morphological characterization of sugar-based hybrid block copolymers (BCPs) consisting of maltoheptaose (MH) and poly(ε-caprolactone) (PCL). The AB-, AB_2-, AB_3-, ABA-, and A_2B-type BCPs, in which the A and B blocks are MH and PCL, respectively, were synthesized by combining the living polymerization and click reaction. The *in-situ* small angle X-ray scattering experiments revealed the formation of ordered microphase-separated structures with a sub-20 nm periodicity.
Keywords: polyester, oligosaccharide, block copolymer, self-assembly

1. Introduction

The self-assembling property of block copolymers (BCPs) to form periodic nanostructures in both the bulk and thin film states has been extensively explored over the past decade for its huge potential to achieve nanopatterning with very small feature size regions of less than 10 nm [1,2]. For such an application, novel BCP systems capable of achieving the well-ordered microphase-separated structures with a sub-20 nm domain-spacing (*d*) are highly desired. The domain-spacing of the microphase-separated structures is described as $d \sim N^{2/3}\chi^{1/6}$, where N is the degree of polymerization and χ is the Flory-Huggins interaction parameter, suggesting that the BCP must have both a low N value and a high χ value to form the microphase-separated structures with a small feature size. Several BCP systems, such as polystyrene-*block*-polydimethylsiloxane [3,4], polystyrene-*block*-poly(2-ethyl-2-oxazoline) [5], polylactide-*block*-polydimethylsiloxane-*block*-polylactide [6], poly(trimethylsilylstyrene)-*block*-polylactide [7], and a poly(methyl methacrylate)-*block*-polyhedraloligomeric silsesquioxane-containing polymethacrylate [8], have achieved the sub-20 nm microphase separation due to the strong segregation between the two constitutional blocks. However, only a limited number of BCPs capable of producing such small features are currently available. Thus, our objective is to develop a new class of so-called "high-χ materials".

Poly- or oligosaccharide-based hybrid BCPs, which have a high χ value due to the strong incompatibility between the hydrophilic saccharidic blocks and hydrophobic synthetic polymer blocks, are some of the promising candidates as high χ-materials for realizing sub-20 nm microphase-separated structures. We previously reported that the hybrid BCPs consisting of polystyrene and malto-oligosaccharides, e.g., maltoheptaose-*block*-polystyrene, were phase separated into ca. 10 nm microdomains by either thermal treatment or solvent annealing in both the bulk and thin film states [9-11]. Such small microdomains were further functionalized by replacing the synthetic polymer block from standard polystyrene by a silicon-containing polystyrene derivative, e.g., maltoheptaose-*block*-poly(4-trimethylsilylstyrene) [12]. The resulting microdomains have a high reactive ion etching contrast between the saccharidic domain and the silicon-containing domain which is highly resistant to oxygen plasma. Thus, it is becoming very important to broaden this class of hybrid BCP systems by integrating a poly- or oligosaccharidic block with functional polymers for potential applications in the nanotechnology field.

Poly(ε-caprolactone) (PCL) is one of the aliphatic polyesters having a biocompatibility and biodegradability. In addition, the crystalline property is also an important characteristic of PCL, which endows its BCPs with interesting phase behaviors associated with its melting or crystallization temperatures (T_m or T_c). When one of the

Received March 29, 2015
Accepted May 11, 2015

blocks consists of sugar, thermal caramelization, i.e., decomposition and/or deformation of the sugar [13, 14], should also affect the self-assembly. Therefore, we synthesized new linear hybrid BCPs consisting of MH and PCL, i.e., MH-*b*-PCL, with different PCL molecular weights, and their microphase separated structures were investigated as a function of the annealing temperature [15].

Furthermore, we were interested in the design and synthesis of nonlinear BCPs consisting of PCL and MH for the fine tuning of their self-assembled morphologies as well as their dimensions. Some pioneering studies on the morphological properties of BCPs with nonlinear architectures, such as macrocyclic BCPs [16], dendritic-linear BCPs [17, 18], $(AB)_n$-type star BCPs [19, 20], and miktoarm star polymers [21, 22], have shown that the nonlinear architecture strongly affected their microphase-separated structures. Among them, the miktoarm star polymers, defined as star-shaped polymers consisting of more than two chemically different polymer chains, have drawn considerable attention because they show unique and unusual morphologies that differ from those of the corresponding linear counterpart. Therefore, we newly designed and synthesized a series of miktoarm star polymers consisting of PCL and MH, from which information about the relationship between the macromolecular architectures and microphase-separated structures were obtained [23, 24].

In this review, our recent results regarding the synthesis and morphological studies of a series of sugar-based hybrid BCPs consisting of PCL and MH (Scheme 1) are summarized.

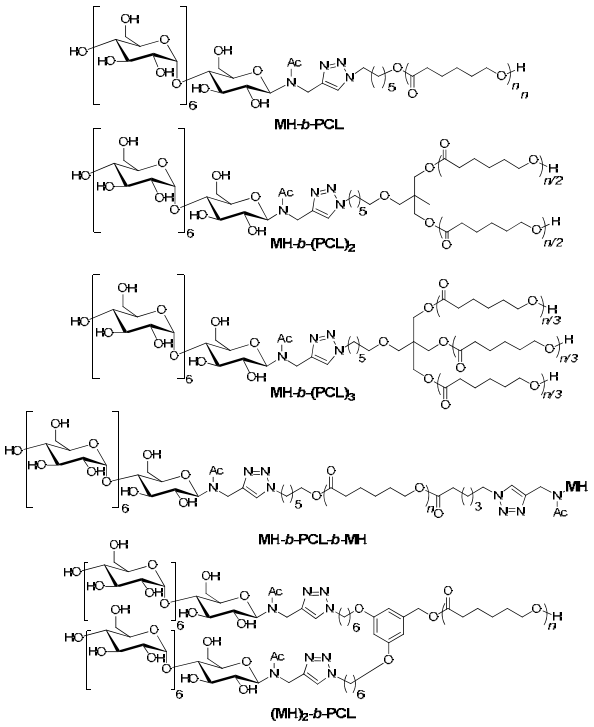

Scheme 1. Hybrid BCPs consisting of PCL and MH

2. Synthesis of Linear and Miktoarm Star BCPs Consisting of PCL and MH

Saccharide-containing BCPs have been produced using several different strategies [25]. Of them, the end-to-end coupling of the saccharidic and synthetic polymer chain ends might be the most effective and simple approaches. Although reductive amination between the reducing end of the saccharide and amino end-functionalized polymer was used as the end-to-end approach, inefficient reaction conditions were required, such as a large excess of saccharide (5 – 100 equivalents) and long reaction time (7 – 8 days) [26, 27]. On the other hand, the click reaction (copper-catalyzed azido-alkyne cycloaddition) has recently emerged as a robust tool for the end-to-end coupling between the ethynyl and azido end-functionalized blocks to produce hybrid BCPs under mild experimental conditions without tedious purifications [28-30]. Indeed, we successfully synthesized sugar-based hybrid BCPs using the click reaction [9, 11, 12]. Therefore, the synthetic strategy for the hybrid BCPs consisting of MH and PCL basically involved the living ring-opening polymerization (ROP) to give the azido end-functionalized PCLs and the subsequent end-to-end coupling with *N*-maltoheptaosyl-3-acetamide-1-propyne (MH-C≡CH) [29] through the click reaction.

Synthesis of MH-b-PCL. Diphenyl phosphate (DPP) was found to effectively catalyze the cationic living ROP of ε-caprolactone (ε-CL) to produce well-defined PCLs with desired end groups that originated from the functional alcohol initiator [31]. Thus, we applied this

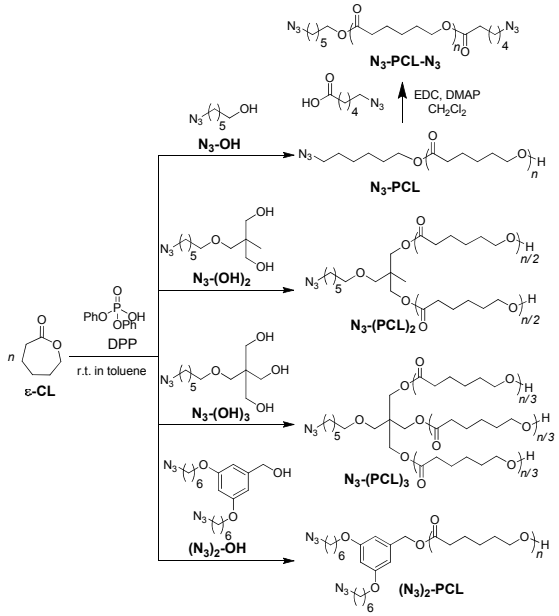

Scheme 2. Synthesis of azido-functionalized PCLs via DPP-catalyzed living ROP

polymerization method to the synthesis of azido end-functionalized PCLs (N_3-PCL) using 6-azidohexanol as the initiator (Scheme 2). By varying the monomer-to-initiator ratio, N_3-PCLs with different M_n values of 2800, 4890, and 10320 g mol^{-1} were prepared for the evaluation of the effect of the molecular weight on their phase behaviors. The click reaction of the N_3-PCLs with 1.3 equivalents of MH-C≡CH was carried out using the CuBr/*N*,*N*',*N*',*N*'',*N*''-pentamethyldiethylenetriamine (PMDETA) catalyst system in DMF at 60 °C to produce the desired MH-*b*-PCLs in good yields (63 – 93%). The success of the click reaction was confirmed by size-exclusion chromatography (SEC), FT-IR, and NMR analyses. Thus, the end-to-end coupling strategy based on the click reaction was found to be effective for the synthesis of the hybrid BCPs consisting of PCL. Note that no chain scission and/or decomposition of the PCL main chain was observed during the click reaction.

Synthesis of MH-b-(PCL)$_2$ and MH-b-(PCL)$_3$. For the synthesis of MH-*b*-$(PCL)_2$ and MH-*b*-$(PCL)_3$, we first prepared the linear and three-branched PCLs bearing an azido group on the chain center (N_3-$(PCL)_2$ and N_3-$(PCL)_3$, respectively) by the DPP-catalyzed ROP with 2-[(6-azidohexyloxy)methyl]-2-methylpropane-1,3-diol (N_3-$(OH)_2$) and 2-[(6-azidohexyloxy)methyl]-2-(hydroxymethyl)propane-1,3-diol (N_3-$(OH)_3$) as the initiators (Scheme 2). Two different molecular weight series of N_3-$(PCL)_2$ (M_n values of 5120 and 10010 g mol^{-1}) and N_3-$(PCL)_3$ (M_n values of 5510 and 10330 g mol^{-1}) were synthesized by varying the monomer-to-initiator ratio. The chemical structure, including the arm number as well as the chain end structure, of the obtained PCLs were identified by NMR and mass spectral analyses. The obtained azido-functionalized branched PCLs were subjected to the click reaction with MH-C≡CH to give the AB_n-type miktoarm star copolymers consisting of PCL and MH, i.e., MH-*b*-$(PCL)_2$ and MH-*b*-$(PCL)_3$, where A and B represent the MH and PCL blocks, respectively. It is worth noting that the click reactions of N_3-$(PCL)_2$ and N_3-$(PCL)_3$ with MH-C≡CH well proceeded to give the corresponding products in high yields despite the greater steric crowding around the reactive azido group rather than the linear N_3-PCL.

Synthesis of MH-b-PCL-b-MH and (MH)$_2$-b-PCL. To incorporate two MH segments into the PCL block, *α*,*ω*-diazido and *α*,*α*-diazido end-functionalized PCLs were first prepared via the DPP-catalyzed ROP (Scheme 2). The *α*-azido end-functionalized PCLs (N_3-PCL), which had been obtained as already described, were treated with 6-azidohexanoic acid in the presence of a condensation agent to give the *α*,*ω*-diazido end-functionalized PCLs (N_3-PCL-N_3; M_n = 5200 and 12000 g mol^{-1}). The quantitative introduction of the azido group at the *ω*-chain end was verified by ^{1}H NMR analysis. For preparation of the *α*,*α*-diazido end-functionalized PCL ($(N_3)_2$-PCL), a new initiator, 3,5-bis(6-azidohexyloxy)benzyl alcohol ($(N_3)_2$-OH), was designed and synthesized. The DPP-catalyzed ROPs of *ε*-CL using $(N_3)_2$-OH as the initiator successfully gave the desired $(N_3)_2$-PCLs with two different molecular weights of M_n = 5600 and 11200 g mol^{-1}. The click reactions of N_3-PCL-N_3 and $(N_3)_2$-PCL with 2.6 equivalents of MH-C≡CH were performed in DMF at 60 °C for 2 days. The completion of the reactions was confirmed by the FT-IR, NMR, and SEC analyses, demonstrating the formation of the desired ABA-type triblock (MH-*b*-PCL-*b*-MH) and A_2B-type miktoarm star copolymers ($(MH)_2$-*b*-PCL) with high purities.

Table 1. Molecular parameters of hybrid BCPs consisting of MH and PCL

sample	$M_{n,PCL}$ [a] (g mol^{-1})	$M_{n,BCP}$ [b] (g mol^{-1})	M_w/M_n [c]	φ_{MH} [d]
MH-*b*-$PCL_{2.5k}$	2800	4030	1.17	0.27
MH-*b*-PCL_{5k}	4890	6120	1.04	0.18
MH-*b*-PCL_{10k}	10200	11550	1.05	0.09
MH-*b*-$(PCL_{2.5k})_2$	5120	6350	1.05	0.18
MH-*b*-$(PCL_{5k})_2$	10010	11240	1.04	0.09
MH-*b*-$(PCL_{1.7k})_3$	5510	6740	1.05	0.18
MH-*b*-$(PCL_{3.3k})_3$	10330	11560	1.05	0.09
MH-*b*-PCL_{5k}-*b*-MH	5200	7660	1.16	0.28
MH-*b*-PCL_{10k}-*b*-MH	12000	14460	1.18	0.15
$(MH)_2$-*b*-PCL_{5k}	5600	8060	1.13	0.27
$(MH)_2$-*b*-PCL_{10k}	11200	13660	1.13	0.16

[a] M_n of the corresponding azido-functionalized PCL was determined by ^{1}H NMR. [b] M_n of the BCP was calculated by summing $M_{n,PCL}$ and molecular weight of MH-C≡CH. [c] Estimated by SEC in DMF containing 0.01 mol L^{-1} LiCl using polystyrene standards. [d] Calculated using d_{MH} = 1.36 g cm^{-3} and d_{PCL} = 1.15 g cm^{-1}.

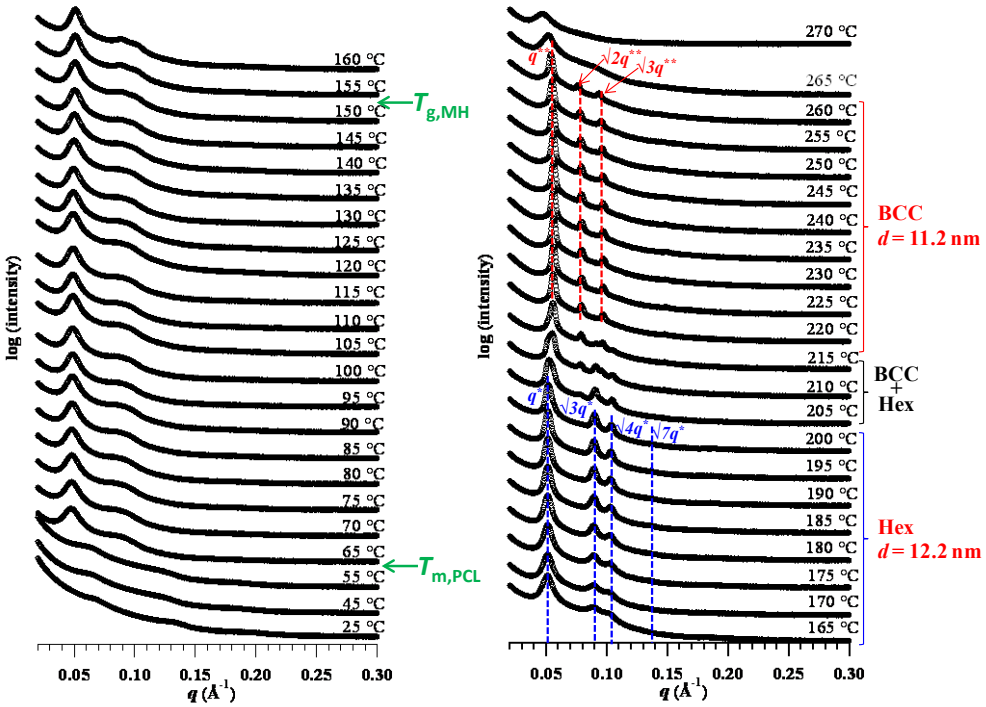

Figure 1. Variation in *in-situ* SAXS profiles of MH-*b*-PCL_{5k} during heating from 25 to 270 °C.

The molecular parameters of all the obtained hybrid BCPs are summarized in Table 1. The MH volume fraction (φ_{MH}) for these BCPs were in the range of 0.08 – 0.27.

3. Microphase-Separated Structures in Hybrid BCP Consisting of PCL and MH

Microphase separation in MH-b-PCL. To evaluate the microphase-separated structure, we employed *in-situ* small angle X-ray scattering (SAXS) and atomic force microscopy (AFM) techniques. The SAXS experiments were performed on the bulk samples of MH-*b*-PCLs with different PCL molecular weights. The SAXS profiles were obtained in real-time using a synchrotron light source during the step-by-step temperature increase. Figure 1 shows the variable temperature SAXS profiles of MH-*b*-PCL_{5k} (φ_{MH} = 0.18) as a representative example, which demonstrated the drastic change in the morphology depending on the annealing temperature. At around room temperature, broad SAXS profiles without any scattering peaks were observed in MH-*b*-PCL_{5k}. Distinct primary scattering peaks (q^*) then appeared when heating above 65 °C corresponding to the melting temperature of the PCL block (T_m of PCL is around 60 °C). The increased mobility of the PCL block induced the self-assembly into thermodynamically stable phases. Higher ordered scattering peaks corresponding to a hexagonally close-packed cylinder (Hex) morphology were observed in the SAXS profiles of MH-*b*-PCL_{5k} obtained in the temperature range of 160 – 200 °C. Thus, we found that the ordered microphase-separated phases were attained by heating above ca. 160 °C corresponding to the glass transition temperature of MH [32]. The domain-spacing (d) of the Hex morphology was calculated to be 12.2 nm using Bragg's equation given by $d = 2\pi/q^*$. Thus, the MH-*b*-PCL system was found to be very effective for constructing sub-20 nm nanostructures. Interestingly, a drastic microphase transition was observed by continuing the heating. In the temperature range of 220 – 260 °C, the SAXS profiles of MH-*b*-PCL_{5k} showed distinct q^{**} and higher order scattering peaks corresponding to a body-centered cubic (BCC) morphology with d = 11.2

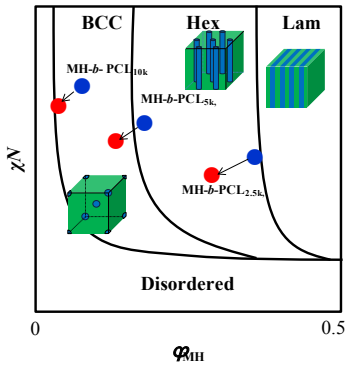

Figure 2. Schematic of the conceptual phase diagram of MH-*b*-PCL system and the phases of MH-*b*-$PCL_{2.5k}$, MH-*b*-PCL_{5k}, and MH-*b*-PCL_{10k} before (bule dot) and after (red dot) thermal caramelization.

nm. Such a phase transition was also visualized by AFM measurements. This phase transition was attributed to the decrease in the effective φ_{MH} due to the thermal caramelization process by heating above 200 °C. MH-*b*-PCL_{5k} should lie close to the phase boundary between Hex and BCC in the phase diagram, and the decrease in the effective φ_{MH} led to the shift in the phase from Hex to BCC.

The *in-situ* SAXS measurements were also performed on the MH-*b*-PCLs with different PCL molecular weights, i.e., MH-*b*-$PCL_{2.5k}$ (φ_{MH} = 0.27) and MH-*b*-PCL_{10k} (φ_{MH} = 0.09), to clarify the effect of φ_{MH} on their self-assembling behavior. For MH-*b*-$PCL_{2.5k}$, the Hex morphology with d = 10.2 nm was observed in the temperature range of 160 – 260 °C. On the other hand, MH-*b*-PCL_{10k} exhibited a BCC morphology with d = 14.0 nm in the temperature range of 135 – 250 °C. Unlike the case of MH-*b*-PCL_{5k}, MH-*b*-$PCL_{2.5k}$ and MH-*b*-PCL_{10k} did not exhibit any microphase transition. MH-*b*-$PCL_{2.5k}$ and MH-*b*-PCL_{10k} should be deeply embedded in the Hex and BCC parts, respectively, and therefore, the slight decrease in the effective φ_{MH} due to caramelization did not affect their morphology. The conceptual phase diagram for the MH-b-PCL system is given in Figure 2.

Microphase separation in MH-b-(PCL)$_2$ and MH-b-(PCL)$_3$. One of our main interests is the morphology control through the design of a macromolecular architecture. Thus, we next investigated the microphase-separated structures of the hybrid BCPs possessing two- or three-branched PCL blocks, i.e., MH-*b*-$(PCL)_2$ and MH-*b*-$(PCL)_3$, whose total PCL molecular weights were fixed at ca. 5000 and 10000 g mol^{-1}, respectively. The *in-situ* SAXS experiments of MH-*b*-$(PCL_{2.5k})_2$ and MH-*b*-$(PCL_{1.7k})_3$ revealed the formation of BCC phases with d values of 9.9 and 9.3 nm, respectively, in the temperature range below ca. 200 °C. It is worth noting that the morphology and d value of the miktoarm BCPs are obviously different from those of the corresponding linear diblock copolymer (MH-*b*-PCL_{5k}) that exhibited a Hex phase with d = 12.2 nm within a similar temperature range. Further heating of these samples led to a decrease in the d value while keeping the BCC phase, which should be attributed to the thermal caramelization of the MH block. As a consequence of the caramelization, the d values for the BCC morphology of MH-*b*-$(PCL_{2.5k})_2$ and MH-*b*-$(PCL_{1.7k})_3$ reached 9.8 and 8.8 nm, respectively (Figure 3). Interestingly, the d values of the BCC morphology were found to decrease by increasing the degree of branching of the PCL block despite the comparable φ_{MH} and molecular weight. A similar tendency was observed among MH-*b*-PCL_{10k} (d = 14.0 nm at 135 – 250 °C), MH-*b*-$(PCL_{5k})_2$ (d = 10.5 nm at 75 – 215 °C), and MH-*b*-$(PCL_{3.3k})_3$ (d = 9.8 nm at 75 – 195 °C). The decrease in d observed in the miktoarm BCPs should be attributable to the decrease in the radius of gyration of the PCL block.

Microphase separation in MH-b-PCL-b-MH and (MH)$_2$-b-PCL. The above-described MH-containing BCPs possessed a small saccharide volume fraction because of the low molecular weight of MH, resulting in the formation of only the Hex and BCC morphologies. Therefore, of particular interest is to construct the other possible morphologies, such as lamellar (Lam) and gyroid, from the MH/PCL BCP system. We expected that the incorporation of multiple MH blocks into the BCP provides a higher φ_{MH} and becomes deeply embedded in the central part of the phase diagram, thus allowing to the formation of the Lam morphology. Therefore, we investigated the microphase-separated structures of MH-*b*-PCL-*b*-MH and $(MH)_2$-*b*-PCL by *in-situ* SAXS experiments. The temperature-dependent SAXS profile of MH-*b*-PCL_{5k}-*b*-MH turned out to be very similar to that of MH-*b*-$PCL_{2.5k}$ (Hex with d = 10.2 nm). Indeed, the SAXS profiles obtained at 160 – 250 °C revealed the formation of a Hex morphology with d = 10.4 nm. In addition, MH-*b*-PCL_{10k}-*b*-MH (Hex with d = 13.1 nm at 160 – 225 °C and BCC with d = 12.4 nm at 235 – 270 °C) and MH-*b*-PCL_{5k} (Hex with d = 12.2 nm at 165 – 200 °C and BCC with d = 11.2 nm at

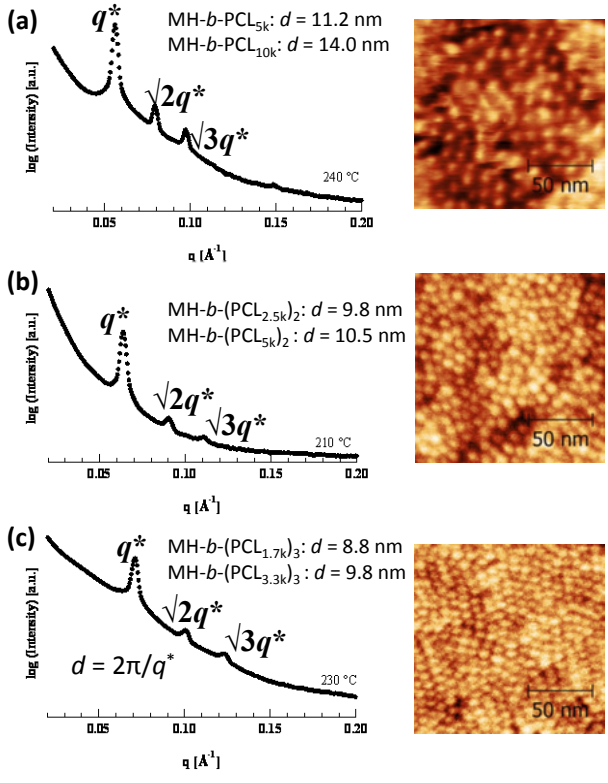

Figure 3. Synchrotron SAXS profiles and AFM images of (a) MH-*b*-PCL_{5k}, (b) MH-*b*-$(PCL_{2.5k})_2$, and (c) MH-*b*-$(PCL_{1.7k})_3$ at selected temperatures.

220 – 250 °C) also exhibited similar microphase-separated structures. Previous studies had revealed that the phase and domain-spacing of the ABA triblock copolymers are almost identical to those of the AB diblock copolymers obtained by cutting the B block at the center [33, 34]. Therefore, the similarity in the microdomain structures between MH-*b*-PCL_{5k}-*b*-MH and MH-*b*-$PCL_{2.5k}$ is consistent with the previous reports. On the other hand, $(MH)_2$-*b*-PCL_{5k} and $(MH)_2$-*b*-PCL_{10k} showed quite different microphase-separated structures as compared to MH-*b*-PCL-*b*-MHs having comparable φ_{MH}s and molecular weights. Indeed, $(MH)_2$-*b*-PCL_{5k} and $(MH)_2$-*b*-PCL_{10k} formed Lam morphologies with *d* values of 17.5 and 21.0 nm, respectively, in the temperature range before starting the thermal caramelization. According to Milner's theory [35], the A_2B-type miktoarm star polymers with $\varphi_A < \varphi_B$ are expected to form a flat interfacial curvature as compared to that of the linear counterpart, which is consistent with the phase behavior of $(MH)_2$-*b*-PCL. The thermal caramelization by further elevating the temperature induced the phase transitions from the Lam to Hex phases with the *d* value of 14.6 nm for $(MH)_2$-*b*-PCL_{5k} and 19.1 nm for $(MH)_2$-*b*-PCL_{10k}. Thus, both $(MH)_2$-*b*-PCL_{5k} and $(MH)_2$-*b*-PCL_{10k} lie close to the phase boundary between the Lam and Hex phases in the phase diagram, resulting in the phase transition to Hex upon thermal caramelization (Figure 4).

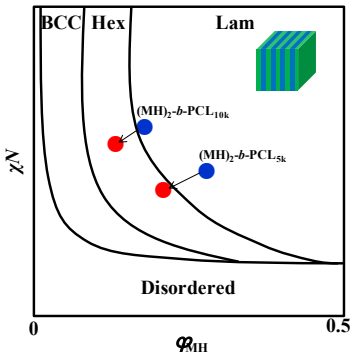

Figure 4. Schematic of conceptual phase diagram and phases of $(MH)_2$-*b*-PCL system before (blue dot) and after (red dot) thermal caramelization.

Relationship between macromolecular architecture and morphology. The BCP self-assembly is mainly governed by the volume fraction of each block, thus leading to various morphologies. In addition to the volume fraction, our results clearly demonstrated that the branched architecture of the BCPs is another important parameter for controlling the morphology and dimensions of the MH/PCL BCP system. Figure 5a summarizes the phase behaviors of MH-*b*-PCL (AB-type), MH-*b*-PCL-*b*-MH (ABA), MH-*b*-$(PCL)_2$ (AB_2), MH-*b*-$(PCL)_3$ (AB_3), and $(MH)_2$-*b*-PCL (A_2B) based on the SAXS results obtained at 190 °C. Note that MH-*b*-PCL-*b*-MH was assumed to be architecturally the same as MH-*b*-PCL because the microdomain structures of both BCPs were in good agreement as already discussed. It was found that the morphology of the MH/PCL BCPs was significantly affected by the branched architecture independent of ϕ_{MH}. For example, the morphology of the BCPs was varied from Lam to BCC upon the changes in the branched architecture with the constant ϕ_{MH} of *ca.* 0.18. Therefore, the macromolecular architecture is a useful tool for obtaining a variety of nanostructures from the MH/PCL BCPs independent of ϕ_{MH}. For the linear BCPs (including MH-*b*-PCL and MH-*b*-PCL-*b*-MH), the observed morphologies shifted from BCC to Hex with the increasing ϕ_{MH}, while the Lam morphology had never been observed. When the A_2B-type branched architecture was utilized, the Lam morphology was observed even though the linear counterparts exhibited a Hex morphology. Thus, placing two MH segments at one end of the PCL block, rather than placing an MH segment at both chain ends of the PCL block, results in a

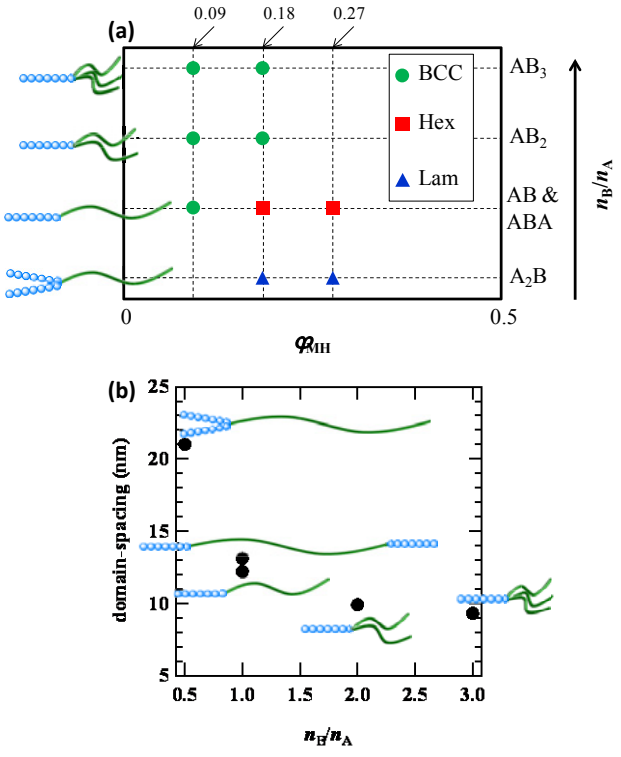

Figure 5. (a) Phase behavior of MH/PCL BCP system, which was determined by the SAXS profiles obtained at 190 °C. (b) Domain-spacing of the morphologies obtained from MH/PCL BCP systems (φ_{MH} = ca. 0.18, temp. = 190 °C) as a function of n_B/n_A, where n_A is arm number of MH block and n_B is arm number of PCL block.

morphology with a lower curvature (Figure 6). MH-*b*-$(PCL)_2$ and MH-*b*-$(PCL)_3$ preferentially formed the BCC morphology, revealing that branching the PCL block into shorter arms results in a morphology with a higher curvature (Figure 6). We found that the *d* value of the morphologies is also affected by the branched architecture. As shown in Figure 5(b), the *d* value decreases with the increasing n_B/n_A value, in which n_A and n_B are the arm numbers of the A (= MH) and B (= PCL) blocks, respectively. Such a control of *d* in the sub-20 nm length scale is one of the attractive features of the MH/PCL BCP system for diverse applications in nanotechnology.

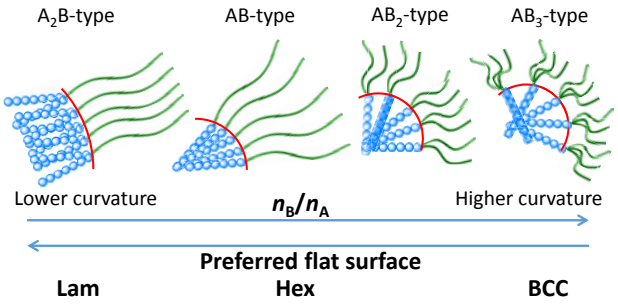

Figure 6. Schematic representation of the relationship between the branched architecture and microphase-separated structure of MH/PCL BCP system.

4. Conclusion

The AB-type linear diblock copolymers consisting of MH (as A block) and PCL (as B block) were successfully synthesized by the click coupling of the azido end-functionalized PCLs and ethynyl end-functionalized MH in high yields. The end-to-end coupling strategy using click chemistry was further expanded to the synthesis of architecturally complex BCPs, such as ABA-, A_2B-, AB_2-, and AB_3-type BCPs(A = MH, B = PCL), through the combination of specially-designed azido-functionalized PCLs. Having a toolbox of various azido-functionalized polymers in hand would allow for creating a wide array of novel saccharide-containing BCP systems.

All the BCPs consisting of PCL and MH with the ϕ_{MH} of 0.08 – 0.27 were found to form microphase-separated structures with a sub-20 nm length scale in the bulk, in which the phase and domain-spacing of the resultant morphologies were highly dependent on the branched architectures. The linear AB-type BCP with the ϕ_{MH} of 0.27 and 0.18 formed a Hex morphology while that with the ϕ_{MH} of 0.08 formed a BCC morphology. The microphase-separated structures obtained from the ABA-type linear triblock copolymers were essentially the same as those of the AB-type counterparts. For the AB_x-type architecture, the domain-spacing of the obtained BCC was found to decrease with the increasing degree of branching for the PCL block. The domain-spacing of the AB_3-type BCP with the $M_{n,PCL}$ of *ca.* 5000 g mol^{-1} was 8.8 nm, which is one of the smallest feature sizes of the microphase-separated BCPs already reported. When compared to the AB-, A_2B-, ABA-, AB_2-, and AB_3-type BCPs with a comparable ϕ_{MH} value of *ca.* 0.16, the domain-spacing decreased with the increasing n_B/n_A value (n_A and n_B are arm numbers of A and B blocks, respectively). The n_B/n_A value was found to be a key factor independent of ϕ_{MH}, which determines the phase as well as the domain-spacing. Such a controllability of the microphase-separated structures with a sub-20 nm length scale is highly intriguing for applications in nanopatterning via BCP lithography.

Acknowledgements

T.S. acknowledges the financial support from the MEXT Grant-in-Aid for Scientific Research on Innovative Areas "Advanced Molecular Transformation by Organocatalysts" and MEXT Grant-in-Aid for Scientific Research (B) (25288093). R.B., I.O., and S.H. thank financial support from CNRS, POLYNAT Carnot, and Labex ARCANE. T.I. is grateful for the financial support from a Grant-in-Aid for Regional R&D Proposal-Based Program from Northern Advancement Center for Science & Technology of Hokkaido Japan.

References

1. Bate, F. S.; Fredrickson, G. H. *Phys. Today,* **52** (1998) 32-38.
2. Kim, J. K.; Yang, S. Y.; Lee, Y.; Kim, Y. *Prog. Polym. Sci.,* **35** (2010) 1325-1349.
3. Son, J. G.; Hannon, A. F.; Gotrik, K. W.; Alexander-Katz, A.; Ross, C. A. *Adv. Mater.,* **23** (2010) 634-639.
4. Jung, Y. S.; Chang, J. B.; Verploegen, E.; Berggren, K. K.; Ross, C. A. *Nano Lett.,* **10** (2010) 1000-1005.
5. Kemp, K.; killops, K. L.; Poelma, J. E.; Jung, H.; Bang, J.; Hoogenboom, R.; Tran, H.; Hawker, C. J.; Schubert, U. S.; Campos, L. M. *Macro Lett.,* **2** (2013) 677-682.
6. Cushen, J. D.; Bates, C. M.; Rausch, E. L.; Dean, L. M.; Zhou, S. X.; Willson, C. G.; Ellison, C. J. *Macromolecules,* **45** (2012) 8722-8728.
7. Rodwogin, M. D.; Spanjers, C. S.; Leighton, C.; Hillmyer, M. A. *ACS Nano,* **4** (2010) 725-732.
8. Hirai, T.; Leolukman, M.; Liu, C. C.; Han, E.; Kim, Y. J.; Ishida, Y.; Hayakawa, T.; Kakimoto, M.-a.; Nealey, P. F.; Gopalan, P. *Adv. Mater.,* **21** (2009)

4334-4338.
9. Aissou, K.; Otsuka, I.; Rochas, R.; Fort, S.; Halila, S.; Borsali, R. *Langmuir* **27** (2011) 4098-4103.
10. Otsuka, I.; Tallegas, S.; Sakai, Y.; Rochas, C.; Halila, S.; Fort, S.; Bsiesy, A.; Baron, T.; Borsali, R. *Nanoscale,* **5** (2013) 2637-2641.
11. Otsuka, I.; Zhang, Y.; Isono, T.; Rochas, C.; Kakuchi, T.; Satoh, T.; Borsali, R. Macromolecules, **48** (2015) 1509-1517.
12. Cushen, J. D.; Otsuka, I.; Bates, C. M.; Halila, S.; Fort, S.; Rochas, C.; Easley, J. A.; Rausch, E. L.; Thio, A.; Borsali, R.; Willson, C. G.; Ellison, C. J. *ACS Nano,* **6** (2012) 3424-3433.
13. Kroh, L. W.; Jalyschko, W.; Hgseler, J. *Starch,* **48** (1996) 426-433.
14. Kroh, L. W. *Food Chem.,* **51** (1994) 373-379.
15. Otsuka, I.; Isono, T.; Rochas, C.; Halila, S.; Fort, S.; Satoh, T.; Kakuchi, T.; Borsali, R. ACS Macro Lett., **1** (2012) 1379.
16. Poelma, J. E.; Ono K.; Miyama, D.; Aida, T.; Satoh, K.; Hawker, C. J. *ACS Nano,* **6** (2012) 10845-10854.
17. Mackay, M. E.; Hong, Y.; Jeong, M.; Tande, B. M. Wagner, N. J.; Hong, S.; Gido, S. P.; Vestberg, R.; Hawker, C. J. *Macromolecules,* **35** (2002) 8391-8399.
18. Lee, E.; Lee, B.-I.: Kim, S.-H.; Lee, J.-K.; Zin, W.-C.; Cho, B.-K. *Macromolecules,* 42 (2009) 4134-4140.
19. Alward, D. B.; Kinning, D. J.; Thomas, E. L.; Fetters, L. J. *Macromolecules,* **19** (1986) 215-224.
20. Herman, D. S.; Kinning, D. J.; Thomas, E. L.; Fetters, L. J. *Macromolecules* **20** (1987) 2940-2942.
21. Khanna, K.; Varshney, S.; Kakkar, A. *Polym. Chem.,* **1** (2001) 1171-1185.
22. Hadjichristidis, N. *J. Polym. Sci. Part A: Polym. Chem.,* **37** (1999) 857-871.
23. Isono, T.; Otsuka, I.; Kondo, Y.; Halila, S.; Fort, S.; Rochas, C.; Satoh, T.; Borsali, R.; Kakuchi, T. *Macromolecules,* **46** (2013) 1461-1469.
24. Isono, T.; Otsuka, I.; Suemasa, D.; Rochas, C.; Satoh, T.; Borsali, R.; Kakuchi, T. *Macromolecules*, **46** (2013) 8932-8940.
25. Schatz, C.; Lecommandoux, S. *Macromol. Rapid Commun.,* **31** (2010) 1664-1684.
26. Bosker, W. T. E.; Ágoston, K.; Stuart, M. A. C.; Norde, W.; Timmermans, J. W.; Slaghek, T. M. *Macromolecules,* **36** (2003) 1982-1987.
27. Yang, Y.; Kataoka, K.; Winnik, F. M. *Macromolecules,* **38** (2005) 2043-2046.
28. Schatz, C.; Louguet, S.; Meins, J.-F. L.; Lecommandoux, S. *Angew. Chem. Int. Ed.,* **48** (2009) 2572-2575.
29. Halila, S.; Manguian, M.; Fort, S.; Cottaz, S.; Hamaide, T.; Fleury, E.; Driguez, H. *Macromol. Chem. Phys.,* **209** (2008) 1282-1290.
30. Otsuka, I.; Travelet, C.; Halila, S.; Fort, S.; Pignot-Paintrand, I.; Narumi, A.; Borsali, R. *Biomacromolecules,* **13** (2012) 1458-1465.
31. Makiguchi, K.; Satoh, T.; Kakuchi, T. *Macromolecules,* **44** (20121) 1999-2005.
32. Imamura, K.; Ohyama, K.-i.; Tani, K.; Yokoyama, T.; Maruyama, Y.; Imanaka, H.; Nakanishi, K. *Spectrosc. Lett,,* **41** (2008) 305-312.
33. Helfand, E.; Wasserman, Z. R. *Macromolecules,* **9** (1976) 879-888.
34. Matsushita, Y.; Nomura. M.; Watanabe, J.; Mogi, Y.; Noda, I.; Imai, M. *Macromolecules,* **28** (1995) 6007-6013.
35. Milner, S. T. *Macromolecules,* **27** (1994) 2333-2335.